Ceramics International 49 (2023) 6834–6842

Contents lists available at ScienceDirect

Ceramics International

journal homepage: www.elsevier.com/locate/ceramint

Preparation and characterization of metakaolin-based geopolymer membrane supports by facile pressed one-part route

Alessandro Filipponi *, Giulia Masi, Serena Bandini **, Maria Chiara Bignozzi

Department of Civil, Chemical, Environmental and Materials Engineering, University of Bologna, via Terracini 28, 40131, Bologna, Italy

ARTICLE INFO

Keywords:
Pressing
Membrane support
Geopolymer
Metakaolin

ABSTRACT

This study reports on the possibility of applying one-part pressed geopolymers as a support for microfiltration membranes. The mineralogical, physical, mechanical, microstructural and hydraulic properties of the investigated materials are presented. Metakaolin-based geopolymeric membrane flat supports were synthesized by uniaxial pressing a dry-mixed powder (Si/Al = 1.45, Na/Al = 0.9, Na/Si = 0.62, H_2O = 12%), with pressure between 2 and 20 MPa and a curing temperature of 70 °C. Mixing and pressing optimization resulted in samples with a total open porosity up to 39%, a modal pore diameter up to 23.5 μm and a flexural strength up to 20.4 MPa. Permeation measurement with demineralized water and ethanol-water solutions were carried out using a dead-end geometry membrane apparatus. A hydraulic permeability up to $31.3{\cdot}10^3$ L h^{-1} m^{-2} bar^{-1} has been obtained. Furthermore, permeation tests using water-ethanol solutions have demonstrated that the material is hydrophilic. These results highlighted the potential of geopolymers as microfiltration support.

1. Introduction

Microfiltration is a membrane separation technique used for many years in many fields such as food, dairy, biotechnology and pharmaceutical industry [1–4]. It comprises different applications: fruit juices clarification, cold sterilization, cell harvesting in continuous fermentation, water treatment in general (post-treatment in activated sludge systems and membrane bioreactors are some examples), pre-treatment of nanofiltration and reverse osmosis steps, water potabilization. Nowadays, asymmetrical membranes, consisting of a support that provides mechanical strength to the membrane without blocking the flow and a selective layer that separates the phases, are largely widespread [5]. Typically, membranes are produced with ceramic or polymeric materials. Most used materials for ceramic membranes are aluminum, zirconium, titanium oxides and silicon carbide [6]. Although the performance of ceramic membranes is very efficient with regards to both durability and selectivity properties, production costs associated with the purchase of pure raw materials and the need of heat treatments frequently lead to their replacement by polymeric membranes [7]. With an average price of 20–200 $ m^{-2}, polymeric membranes are considerably cheaper than ceramic membranes (average costs of 500–3000 $ m^{-2}) [8–10]. On the contrary, with alkali activated materials and geopolymers, membranes could be synthesized with physical and durability properties similar to ceramics, but with lower production costs. Indeed, unlike ceramic materials, geopolymers do not require high-temperature sintering, but they can be cured at temperatures below 100 °C [11].

Geopolymers are made of amorphous aluminosilicate source (such as metakaolin) and activator (such as sodium hydroxide and/or sodium silicate). The activator can be liquid or solid and in the latter case, the system is defined “one-part geopolymers” and the activation reaction starts with the addition of water [12,13]. The application of one-part geopolymers reduces the issue of handling large quantities of hazardous and corrosive alkaline solutions (sodium and potassium silicates and hydroxides) and the environmental impact mainly related to the use of sodium silicate solution generally produced by Solvay process. Furthermore, it has been observed that compressive strength of one-part geopolymers can reach high values, up to 80 MPa. However, despite all these advantages, studies about one-part geopolymers applications are rather limited and mainly addressed to durability, efflorescence phenomena and shrinkage properties [12].

Geopolymers are very versatile as they can be formed by casting, pressing or extrusion methods and used for different applications

* Corresponding author.
** Corresponding author.
E-mail addresses: a.flipponi@unibo.it (A. Filipponi), giulia.masi5@unibo.it (G. Masi), serena.bandini@unibo.it (S. Bandini), maria.bignozzi@unibo.it (M.C. Bignozzi).

https://doi.org/10.1016/j.ceramint.2022.10.233
Received 5 August 2022; Received in revised form 4 October 2022; Accepted 18 October 2022
Available online 20 October 2022

[14–22]. Independently of the applied casting method, geopolymers have an inherent porosity generated by air bubbles in the slurry (macropores, > 10 μm), unreacted particles (meso- and micropores, 100 nm - 10 μm), interstices in the gel (2–100 nm) [23]. If porosity and pore size distribution need to be specifically tailored, methods such as direct foaming, replica, sacrificial filler and 3D printing can be also used. The direct foaming technique is currently the simplest and fastest way, also applicable to one-part geopolymers, to obtain highly porous geopolymers [23,24].

In the scientific literature, few studies already report the synthesis of geopolymeric membranes, both symmetrical (self-sustained) and asymmetrical (support and selective layer) for water filtration, gas separation [25,26] and pervaporation [27,28]. Although symmetrical membranes are not widely industrially produced, good results have been obtained in the filtration of aqueous solutions containing alcohol [28], methylene blue [29], heavy metals [30,31], Na^+ ions [32], oil-water emulsions [33] and nano-particles [34]. With regard to asymmetric membranes, a hybrid membrane has been developed with a metakaolin-based geopolymeric support formed by casting and a selective polymeric layer of chitosan [35]. A cast geopolymeric support based on metakaolin has also been developed by Bai and Colombo by direct foaming method [36]. Porosity was achieved by adding a combination of hydrogen peroxide (H_2O_2) and surfactant to the slurry, achieving a total open porosity of about 65%, a pore size distribution between 100 and 600 μm and a compressive strength of about 4.5 MPa. A similar approach has been used by Xu et al. [37], who developed an asymmetric metakaolin-based membrane by casting for the purification of pulp-papermaking green liquor. The support has a pure water permeability of $133{\cdot}10^3$ kg m^{-2} h^{-1} bar^{-1}, an open porosity of 69.5% and a compressive strength of 4.3 MPa.

The aim of this study has been to understand the applicability of one-part geopolymer materials as supports for water microfiltration. So far, the scientific literature on this topic is scarce and a press-formed geopolymeric membrane supports have never been studied. The support has been developed to be used as flat membranes and the methodology has been optimized in order to obtain a material with high mechanical strength. Based on a previous study [15] where the influence of different Na/Al ratio and water content on microstructural and physical properties of one-part geopolymers was investigated, a mix design was selected and disk-shaped membrane supports were prepared varying the pressures (from 2 up to 20 MPa) during forming. Structural (XRD and FT-IR analyses), physical (bulk density, total open porosity and pore size distribution), mechanical (flexural strength by three-point bending test) and microstructural properties have been determined as function of the applied pressure. Moreover, permeation measurements with demineralized water and ethanol-water solutions have been also carried out on the developed geopolymer membrane supports in order to evaluate their performances and the peculiar characteristic of the “threshold pressure” has been highlighted.

2. Material and methods

2.1. Materials

Flash calcined metakaolin was supplied by Argeco Développement (France). The chemical and mineralogical compositions of metakaolin are reported in a previous study [15]. Anhydrous sodium metasilicate, supplied by Alfa Aesar, was used as activator for the geopolymer synthesis. Permeation tests were performed using demineralized water (21 μS/cm at 24 °C) and water-ethanol solutions at concentrations of 100 and 200 g L^{-1} of ethanol. Ethanol with a purity ≥99.8% has been supplied by Alfa Aesar.

2.2. Samples preparation

Metakaolin and anhydrous sodium metasilicate were dry mixed to obtain a powder mix with the following molar ratios: Si/Al = 1.45, Na/Al = 0.90, and Na/Si = 0.62. Then, the dry mix was sprayed with 12 wt% of demineralized water and formed by uniaxial pressing. Disk-shaped samples (d = 45 mm, h = 2 mm) and prisms (70 mm × 10 mm × 7 mm) were obtained by forming pressures of 2, 5, 10, and 20 MPa (Fig. S1). Samples curing was carried out at 70 °C for 24 h and at room temperature for the following 6 days, keeping the samples sealed in plastic bag to prevent fast water evaporation and consequently crack formation. In order to ensure the planarity of surfaces, all the samples were cured under a 200 g load.

Samples were named as S followed by the applied forming pressure (2, 5, 10, and 20). Any other sample specification, such as the fluid used during permeation tests (PW for pure water and ET for ethanol-water solutions) was added when needed.

2.3. Characterization

2.3.1. Structural, physical, microstructural and mechanical characterization

Structural and mineralogical characterizations were performed using an X-ray diffractometer (XRD, Panalytical Empyrean) equipped with a CuKα tube (λ = 1.5406 Å) operating at 40 kV and 30 mA. Analyses were performed on dried powder (milled samples) using a 2θ range from 4 to 80° and a step size of 0.026°. FT-IR spectra were recorded on powder samples by a Fourier Transform Infrared spectroscopy (FT-IR, PerkinElmer Spectrum One spectrometer) in wavenumber range of 400–4000 cm^{-1} with a resolution of 4 cm^{-1}.

The geometric density (ρ) was calculated by dividing the dry mass of disk-shaped sample by its volume. The total open porosity (φ), pore size distribution and modal pore diameter (D) were determined using a mercury intrusion porosimeter (Pascal 140 and Pascal 240, Thermo Scientific) capable of measuring the volume of pores with diameters in the range between 0.0074 and 116 μm. Testing samples have about 1 cm^3 volume and setting parameters were as follows: contact angle of 141.3° and a Hg surface tension of 480 dyne/cm.

The three-point bending test has been carried out using a universal testing machine (10/M, MTS/US) applying a roller span of 60 mm and a crosshead speed of 5 mm min^{-1}. Flexural strength (σ_f) was calculated using Eq. (1):

$$\sigma_f = \frac{3FL}{2hw^2} \quad (1)$$

where F is the maximum load, L is the length of the support span, w and h are the width and the thickness of the sample, respectively. Flexural strengths reported are the average of five measurements.

Microstructural observations have been performed using a field emission gun scanning electron microscope (FEG-SEM, Tescan Mira3). Samples were coated by graphite using a Quorum sputter coater (Q150R ES) to make them conductive.

2.3.2. Permeation testing apparatus and procedure

Permeation measurements with pure water and water-ethanol solutions were conducted on disk-shaped geopolymer samples using a dead-end geometry apparatus (Sartorius SM165 26 with a maximum capacity of 200 mL) applying a transmembrane pressure (ΔP) between 0.2 and 0.5 bar (Fig. 1, Fig. S2). The permeate is maintained at atmospheric pressure (P_{atm}) while the ΔP (= P_{PI-2} - P_{atm}) is regulated and kept constant via the V-1 valve. The solution charge is 200 mL and the permeate is taken continuously, measuring the volume of permeate over time. Before starting the permeation measurements, all samples were fluxed at 0.5 bar with a volume of water of approximately 7 L. This conditioning was needed to remove unreacted sodium metasilicate, being responsible of a pH increase of permeate up to 12. Fluxing ended when the pH values of feed and permeate were equal, this typically occurring at pH = 6. Finally, samples were dried at 100 °C for 24 h. Transmembrane flux

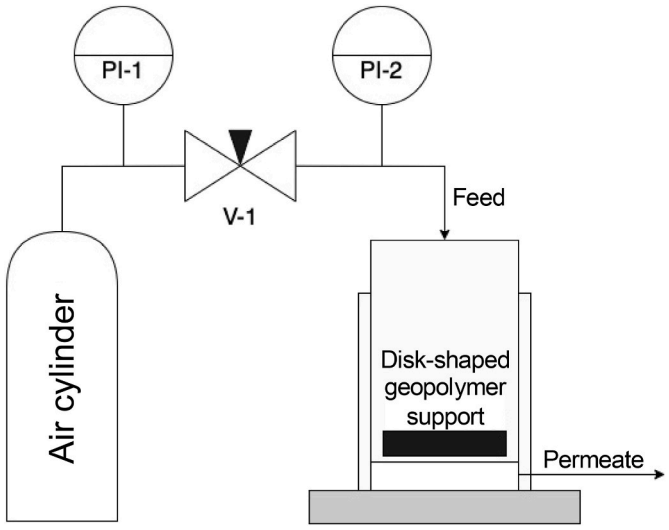

Fig. 1. Dead-end geometry apparatus scheme (PI = Pressure indicator, V = Valve).

measurement was performed applying decreasing pressures, using demineralized water (PW) and ethanol-water solutions (ET100 and ET200), both at room temperature (24 °C). At each pressure value, 9 flow measurements were carried out, with the tank being refilled every 3 measurements to avoid deviations related to the water level. Flux measurements were repeated at least three times and the corresponding standard deviations are reported.

The total volume flux (J_V) was calculated according to Eq. (2):

$$J_V = \frac{V_P}{\Delta t \; A_m} \tag{2}$$

in which V_P represents the permeate volume collected in the time interval Δt and A_m is the area of the disk-shaped geopolymer sample. Experimental data of J_V are reported along the pressure difference ΔP.

3. Results and discussion

3.1. Structural, physical, microstructural and mechanical properties

All the pressed one-part geopolymer samples were tested after 7 days of curing. FT-IR spectra of metakaolin and geopolymer supports were obtained over a scan range of 400–4000 cm^{-1} (Fig. 2). The main band at 1052 cm^{-1} representing the Si–O–Si and Si–O–Al stretching vibration [38–40] is visible in MK spectrum. A shift of this band to 987 cm^{-1} occurs as a consequence of the chemical reorganization and polycondensation due to the geopolymerization reaction for S2, S5, S10 and S20 [41,42]. This shift agrees with what is found for geopolymers prepared by alkaline solutions by Rovnaník et al. [40] and Li et al. [43], which report this band at 1000 cm^{-1} and between 950 and 960 cm^{-1}, respectively. Moreover, whereas in all the spectra, bands between 400 and 800 cm^{-1}, related to the presence of quartz [44], are evident, the band at 1458 cm^{-1}, corresponding to the stretching vibrations of O–C–O bonds [45], occurs only in geopolymer samples. Such vibrations can be associated to the presence of sodium carbonates as a result of carbonation of unreacted sodium silicate. Comparing the four geopolymers spectra, it can be observed that sample S20 is the one with the least intense carbonate band and the most intense peak at 987 cm^{-1}, thus indicating the highest degree of geopolymerization.

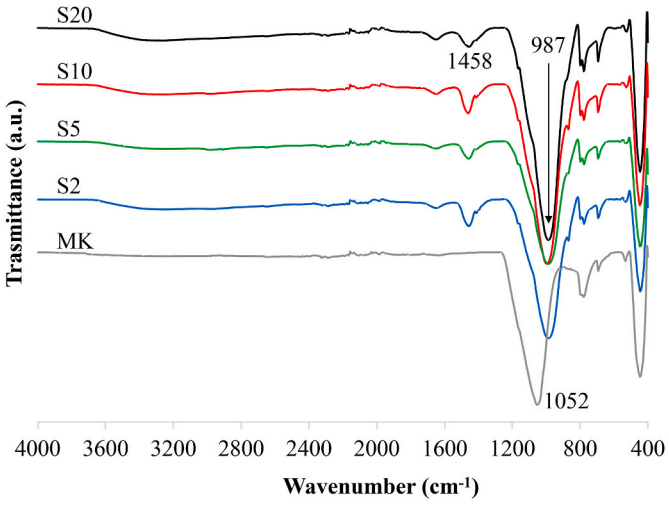

Fig. 2. FT-IR spectra of metakaolin (MK) and geopolymer supports (S2, S5, S10 and S20).

Fig. 3 shows the XRD pattern of the metakaolin and the geopolymer supports S2 and S20. The MK pattern indicates that metakaolin contains mainly quartz (SiO_2) and kaolinite ($Al_2Si_2O_5(OH)_4$) as crystalline phases. The halo peak visible between 20 and 30° represents the amorphous phase typical of aluminosilicate glasses. Pouhet et al. estimated the percentage of amorphous silica for MK supplied by Argeco (the same used in this study), equal to 29%, the rest of SiO_2 being present in the crystalline form of quartz [46]. The broad halo peak shifts to higher 2θ degree values (25–35°) in S2 and S20 spectra, thus exhibiting the same behavior of geopolymers obtained by alkaline solutions. XRD patterns of S2 and S20 also show, in addition to all the phases determined in MK, newly formed peaks attributable to sodium carbonate. This compound is formed by carbonation of unreacted sodium silicate present in the

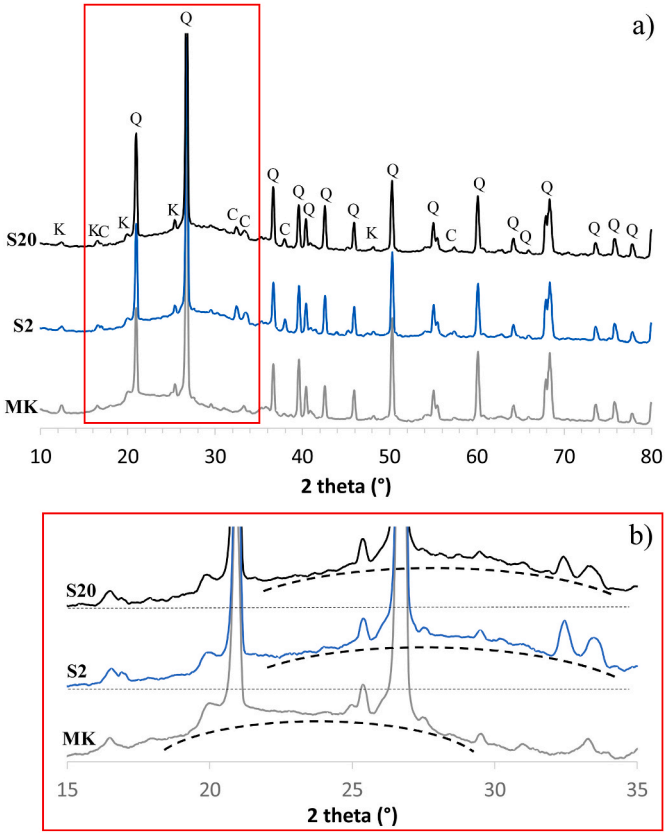

Fig. 3. In a) XRD patterns of metakaolin (MK) and geopolymer supports S2 and S20. Q = quartz, C = sodium carbonate, K = kaolinite. In b) the magnification of the XRD pattern between 15 and 35° showing the position of the broad halo peak.

geopolymer support as already observed by FT-IR spectra. Sodium carbonate peaks are less pronounced in sample S20, highlighting a higher degree of geopolymerization compared to S2.

Finally, apart from sodium carbonate, no other newly formed crystalline phases such as zeolites have been determined in geopolymers spectra, thus indicating that the process parameters set up for the synthesis are suitable as confirmed by both XRD and FT-IR analysis.

In Fig. 4, the results of geometric density and flexural strength are reported. By increasing the forming pressure, both geometric density and flexural strength increased with an exponential trend from 1.54 to 1.88 g cm^{-3} and from 7.3 to 20.4 MPa, respectively.

Flexural strength of the investigated samples can be compared with literature data. Both Obada et al. and Bouzid Rekik et al. report of ceramic supports, based on kaolin clay as raw materials, with a slightly higher flexural strength of about 28 MPa [47,48], while Lorente-Ayza et al. achieved a flexural strength of 39.7 MPa [49]. Jedidi et al., using fly ash as raw material, obtained a support with a slightly lower flexural strength (22.9 MPa) than the one exhibited by S4 [50]. Conversely, considering supports based on pure oxide ceramics (e.g.: α-Al_2O_3 and TiO_2), flexural strength values in the range of 28–87 MPa have been reported in several studies [51–54].

Fig. 5 reports the cumulative open porosity and modal pore diameter determined by mercury intrusion porosimetry. It is observed that by increasing the forming pressure from 2 to 20 MPa the total open porosity decreases from values of 39 to 14%. The modal diameter follows the same trend, showing a decrease from 23.5 to 5.8 μm. Compared to ceramic membrane supports, geopolymer supports generally show a lower cumulative open porosity and a larger pore diameter. Typical values of cumulative open porosity for ceramic supports range between 31 and 51%, while in terms of pore size distribution, typical values are between 0.9 and 16 μm [49–55]. Such variations can be ascribed to raw materials, different consolidation process (ceramics are sintered), and high forming pressure (for ceramic up to 240 MPa [56]).

The differential pore size distribution (Fig. 5) shows that pore dimension of the samples has monomodal curves with narrow distributions. Indeed, increasing forming pressures, denser, more compact and mechanically resistance microstructures are obtained for the investigated mix design. Among the tested disks, S2, S5 and S10 samples pressed at 2, 5 and 10 MPa, respectively, are the more promising in terms of open porosity values and pore size characteristics to serve as a membrane support [6,57].

The FEG-SEM micrographs are reported in Fig. 6 showing the unpolished cross-sections of the synthesized geopolymer supports after 7 days of curing. The porosity characterizing the different samples previously discussed are clearly visible in the reported micrographs and an increasingly dense matrix is observed moving from sample S2 to sample

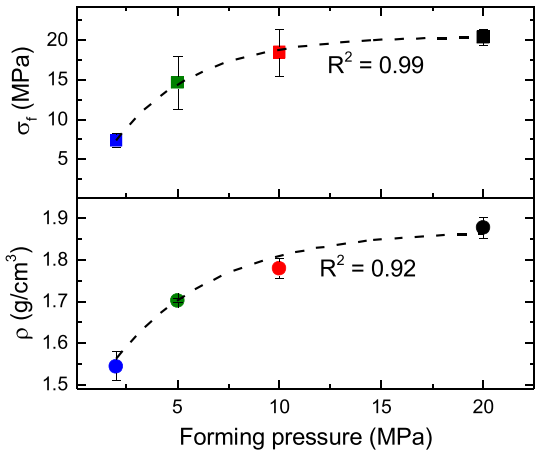

Fig. 4. Flexural strength (σ_f) and geometric density (ρ) of the investigated geopolymeric supports.

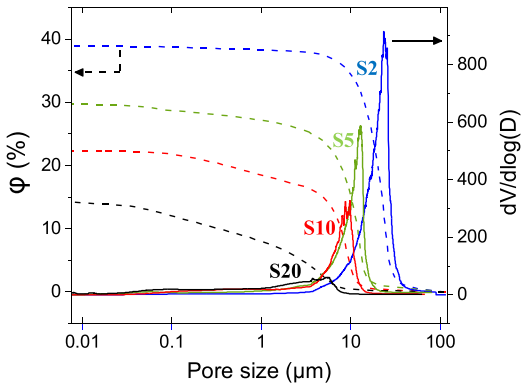

Fig. 5. Cumulative open porosity (φ) and differential pore size distribution (dV/dlog(D)) of the investigated samples.

S20. Furthermore, it can be also noted that the observed samples do not show any macro- or micro-cracks, that may affect geopolymers [58–60], and that the pores are randomly shaped. Fig. 7 shows two micrographs reporting the raw metakaolin and sample S10. Whereas MK is formed by particles mainly constituted by clusters of flakes, geopolymer microstructure is smooth, dense and continuous.

3.2. Membrane permeability

In order to obtain a reliable assessment of permeation features of the investigated samples, filtration tests with pure water and ethanol-water solution were performed on geopolymer supports. Figs. 8–10 show the total volume fluxes (J_v) as a function of the pressure difference across the geopolymer disk (ΔP) obtained for S2, S5, S10 and S20 samples.

Firstly, it can be observed that all the tested supports show a linear trend between the volumetric flux and the transmembrane pressure, with a negative intercept at $\Delta P = 0$; the values of slope and intercept are reported in Figs. 8–10.

In agreement with previous observations, data have been elaborated according to the porous flow law proposed by Huang et al. [61], as reported in Eq. (3). Such equation describes the flow of a liquid in small pore size porous media, as it was observed in the case of rock cores oil reservoir, and reconfirmed by Yin at al. in α-Al_2O_3 membrane supports [53]:

$$J_V = \frac{k_D}{\eta \delta_m}(\Delta p - \Delta p_T) = Per\ (\Delta p - \Delta p_T) \quad (3)$$

In Eq. (3) k_D is the Darcy's permeability coefficient which typically collects the geometrical parameters of the membrane, such as void fraction or interconnected porosity, pore size distribution and tortuosity factor, η represents the dynamic viscosity of the fluid inside the pores and δ_m is the membrane support thickness; the membrane permeability with the testing fluid, *Per,* is defined straightforwardly. Generally speaking, in the case of laminar flow across cylindrical pores of the same pore radius, the Darcy coefficient can be expressed as $k_D = \varphi\ r_p^2/8\tau$, in which r_p represents the pore radius and τ the tortuosity factor, respectively. Since membranes typically shows a pore size distribution and the shape is not cylindrical nor slit-like, that expression can give only an indication of the role of the porosity and pore diameter on the permeability.

With regards to Eq. (3), the flow of a liquid deviates from Darcy's linear law: the so-called threshold pressure difference, Δp_T, should be overcome to allow the liquid flow across the pores. As the pore radius decreases, liquid-solid interactions (intermolecular forces at the liquid-solid interface) increase the liquid viscosity of the fluid close to the pore wall with respect to the viscosity of the bulk fluid. As a consequence, the liquid viscosity is not constant along the pore radius and a non-Newtonian behavior is observed, rather similar to a Bingham fluid

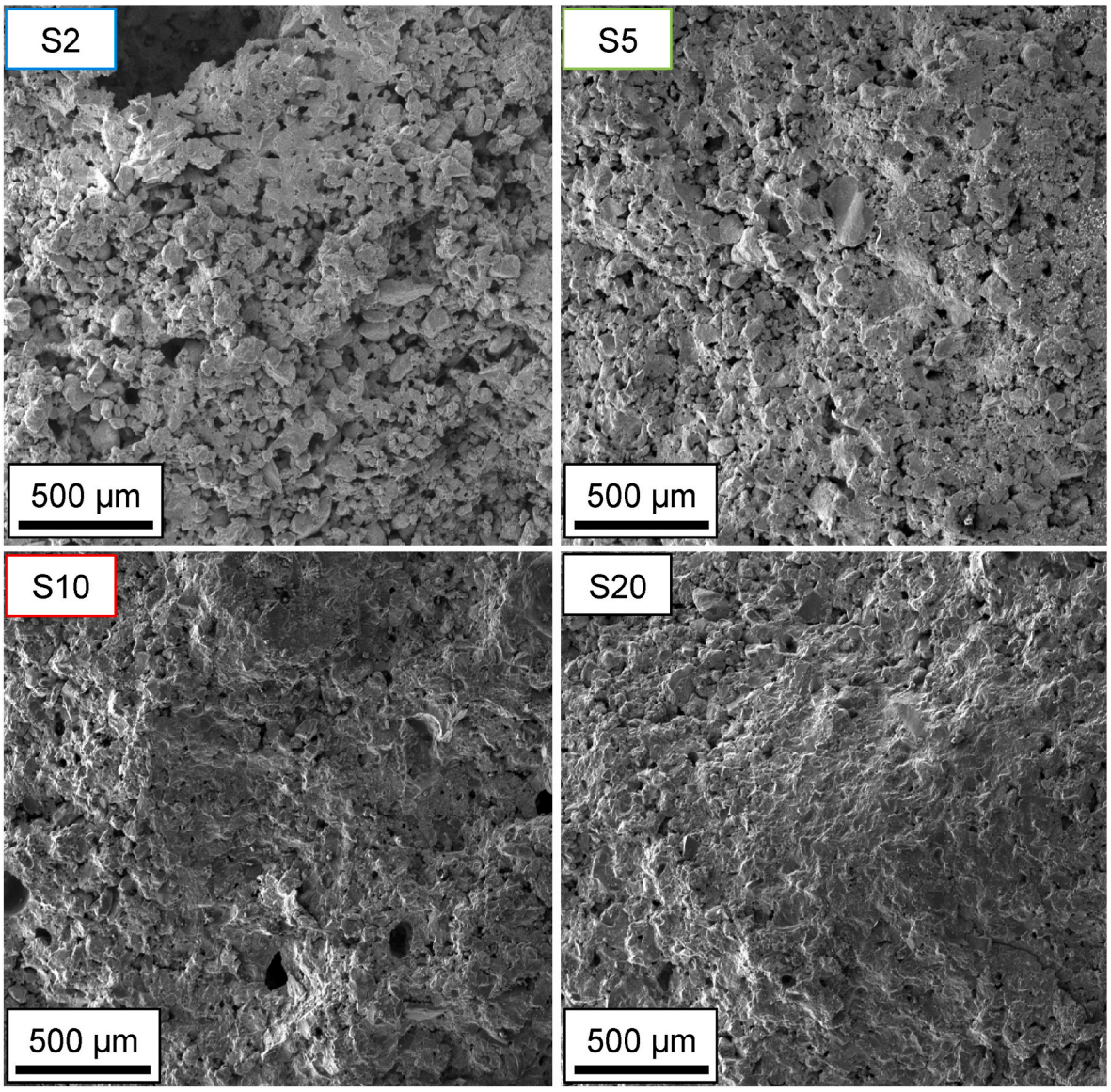

Fig. 6. FEG-SEM micrographs of S2, S5, S10, S20 samples.

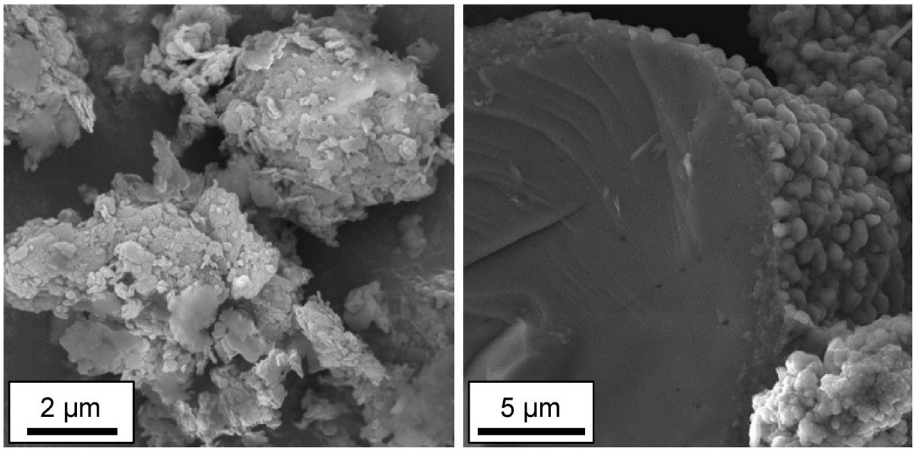

Fig. 7. FEG-SEM micrographs of raw metakaolin (left) and sample S10 (right).

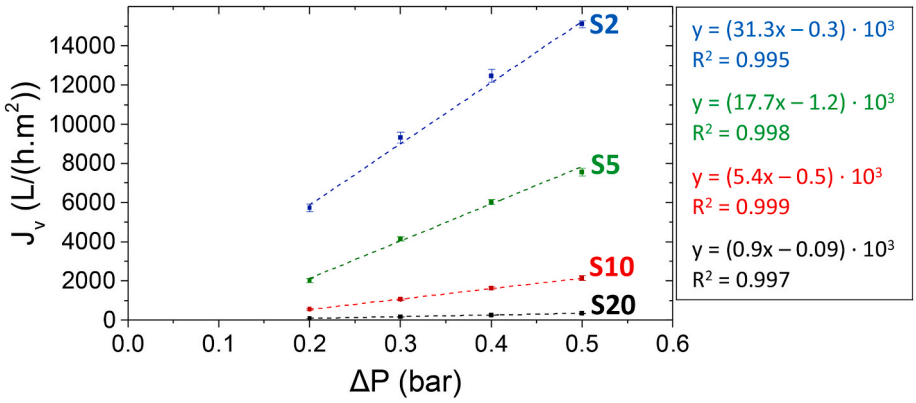

Fig. 8. Transmembrane volume fluxes with pure water at 24 °C of S2, S5, S10, S20 samples as function of ΔP.

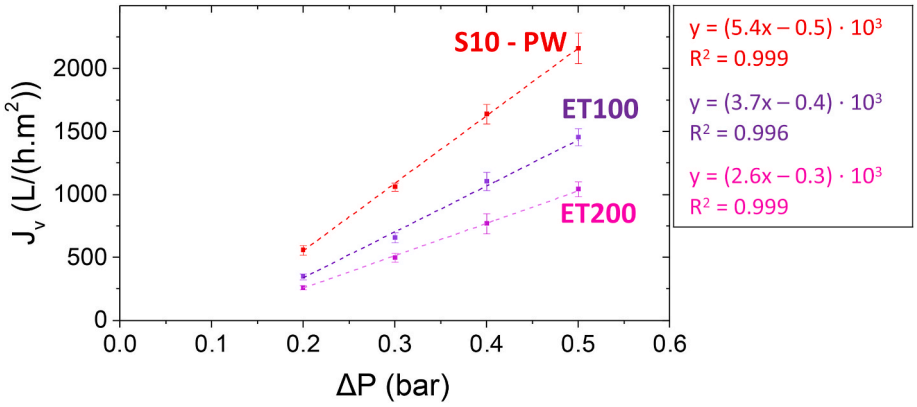

Fig. 9. Transmembrane volume fluxes with pure water and ethanol-water solutions (ethanol concentration of 100 and 200 g L^{-1}) of S10 sample as function of ΔP.

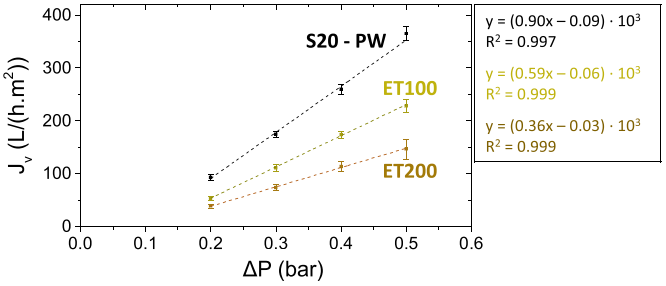

Fig. 10. Transmembrane volume fluxes with pure water and ethanol-water solutions (ethanol concentration of 100 and 200 g L^{-1}) of S20 sample as function of ΔP.

[61]: a minimum activation pressure, the threshold pressure difference (Δp_T), is then necessary to have a liquid flow across the pore. As the pore radius increases, on the contrary, Δp_T decreases, and Eq. (3) degenerates into the typical Darcy's law.

The values of membrane permeabilities of the investigated samples and the corresponding threshold pressures are reported in Table 1 together with the same data determined by Yin et al. [53] for α-Al_2O_3 ceramic support. Data from reference 53 have been selected for comparison's sake.

Increasing the forming pressure from 2 to 20 MPa results in a reduction of the hydraulic permeability (PW data) from values of about $31.3 \cdot 10^3$ to values of about $0.90 \cdot 10^3$ L h^{-1} m^{-2} bar^{-1} (Fig. 8). S2 and S5 samples with permeability values of $31.3 \cdot 10^3$ and $17.7 \cdot 10^3$ L h^{-1} m^{-2} bar^{-1}, respectively, show very promising permeability properties for being used as membrane supports. Although S10 has a lower permeability ($5.4 \cdot 10^3$ L h^{-1} m^{-2} bar^{-1}) compared to S2 and S5 samples, it can still be a valuable support considering its high flexural strength.

Table 1
Physical characteristics (D: modal pore diameter, φ: total open porosity, δ_m: thickness) and transport parameters with pure water (PW) and ethanol-water solutions (ET) (Per: permeability, ΔP_T: threshold pressure) of the investigated samples.

Sample	D (μm)	φ (%)	δ_m (mm)	Fluid	*Per* (L/(h.m².bar)) · 10^3	ΔP_T (mbar)	Per_w/Per_{Et}	Reference
S2	23.5	39	2	PW	31.3 ± 0.8	9 ± 18	–	This work
S5	12.7	30	2	PW	17.7 ± 0.6	66 ± 12	–	
S10	9.8	22	2	PW	5.4 ± 0.3	99 ± 14	–	
				ET-100	3.7 ± 0.2	119 ± 24	1.46	
				ET-200	2.6 ± 0.2	105 ± 22	2.08	
S20	5.8	14	2	PW	0.90 ± 0.1	104 ± 20	–	
				ET-100	0.59 ± 0.03	105 ± 16	1.53	
				ET-200	0.36 ± 0.02	92 ± 22	2.50	
α-Al_2O_3	4.6	31	3.5	PW	17.9	93	–	[53]

As with typical ceramic or polymeric microfiltration supports, hydraulic permeability of the investigated samples decreases with decreasing pore diameter and total open porosity, in complete agreement with the Darcy law. Indeed, the most porous support (S2) with a total porosity of 39% and a modal pore size of 23.5 μm has a hydraulic permeability of $31.3{\cdot}10^3$ L h^{-1} m^{-2} bar^{-1}; in contrast, the least porous support (S20), with a total open porosity of 14% and a modal pore size of 5.8 μm has a permeability of $0.9{\cdot}10^3$ L h^{-1} m^{-2} bar^{-1}. Similar hydraulic permeability values ($18{\cdot}10^3$ and $7.6{\cdot}10^3$ L h^{-1} m^{-2} bar^{-1}) were obtained from supports made of α-Al_2O_3 by Yin et al. and Qin et al. [53,55] with porosity and pore size of 31 and 46%, 3.5 and 4.7 μm, respectively. A permeability of $13{\cdot}10^3$ L h^{-1} m^{-2} bar^{-1} was also achieved using traditional ceramic membranes (kaolin and calcium carbonate as raw materials), creating a support with a porosity of 47% and an average pore size of 8 μm [62]. Aouadja et al. [51] have achieved an excellent permeability of $15.7{\cdot}10^3$ L h^{-1} m^{-2} bar^{-1} with a porosity of 46% and a pore size of 7.7 μm from a diatomite/alumina mixture as raw material. Another extremely high permeability value ($45{\cdot}10^3$ L h^{-1} m^{-2} bar^{-1}) was obtained with a support with 41% of open porosity and 6.8 μm pore size.

With regards to the threshold pressures (Table 1) it can be seen that increasing the forming pressure (samples S2 to S20) leads to an increase in Δp_T from 9 mbar to 104 mbar, when using pure water. This means that the Δp_T increases as the porosity and modal pore size decrease. Such behavior indicates the presence of a strong fluid-solid interaction inside the pores with a corresponding increase of the viscosity close to the fluid/solid interface. This is indicative of a considerable affinity of the support for water, confirming the hydrophilic character of the geopolymer. Finally, it can be observed that the Δp_T values calculated for the samples S10 (99 mbar) and S20 (104 mbar) are in a very good agreement with the value (93 mbar) obtained by Yin et al. [53] for α-Al_2O_3 membranes.

With regard to permeability with ethanol-water solutions, a decrease in permeability with increasing ethanol concentration is observed for both samples S10 (Fig. 9) and S20 (Fig. 10), (see also Table 1). S10 shows a reduction of permeability from about $5.4{\cdot}10^3$ to $2.6{\cdot}10^3$ L h^{-1} m^{-2} bar^{-1} when the ethanol concentration increases from 0 to 200 g L^{-1}. S20 exhibit the same trend with permeability values that ranges from $0.9{\cdot}10^3$ to $0.36{\cdot}10^3$ L $h^{-1}m^{-2}$ bar^{-1}. Only the results of samples S10 and S20 are reported, since the corresponding data show lower standard deviations both on fluxes and on the Δp_T than the cases of samples S2 and S5 (Table 1), allowing more precise evaluations.

As the threshold pressure values with ethanol solutions, the calculated Δp_T do not assume any remarkable trend, with values always like those obtained with pure water, although a slight decrease can be evidenced as the ethanol concentration increases. That behavior might suggest that the fluid-solid interactions at the pore wall slightly decrease, due to the hydrophilic character of the membrane material.

Finally, it should be observed that the decrease in permeability with ethanol-water solutions is mostly related to the greater value of the bulk viscosity of ethanol-water solutions with respect to the pure water value: at 20 °C viscosity of 100 g L^{-1} and of 200 g L^{-1} ethanol-water solutions is 1.51 mPa s and 2.18 mPa s, respectively, with respect to the pure water viscosity of 1.0 mPa s. Considering Eq. (3), assuming the same values of k_D and δ_m, the ratio of the permeabilities of pure water and ethanol-water solutions, Per_w/Per_{Et}, should correspond to the bulk viscosity ratio. Indeed, this ratio is evaluated as 1.46 and 1.53 for ET-100 and 2.08 and 2.50 for ET-200, for samples S10 and S20 respectively (Table 1). Apparently, Eq. (3) is a very good representation of the behavior of geopolymer support.

As a final comment, it is interesting to observe that permeation measurements were repeated at least three times obtaining very reproducible results, exhibiting small standard deviation values. The applied mix design and forming method allowed the synthesis of samples with reproducible characteristics.

4. Conclusions

In this study, membrane supports for water microfiltration were successfully synthesized by pressing one-part geopolymers. Based on the obtained results, conclusive observations can be made as follows:

- preparing one-part geopolymers by pressing makes possible to obtain high permeability supports (up to $31.3{\cdot}10^3$ L h^{-1} m^{-2} bar^{-1}) that are hydrophilic and with a total open porosity and a modal pore size up to 39% and 23.5 μm, respectively. In addition, the permeabilities obtained with geopolymer supports are similar to those obtained with ceramic supports;
- geopolymer supports possess a characteristic threshold pressure that increases with the lowering of their porosity and pore size;
- the synthesized geopolymeric supports show high mechanical strength which is correlated to the forming pressure. A maximum flexural strength of 20.4 MPa has been achieved when the applied forming pressure is equal to 20 MPa. S10 sample, which shows good permeability results ($5.4{\cdot}10^3$ L h^{-1} m^{-2} bar^{-1}), has a flexural strength of 18.5 MPa;
- among the prepared geopolymeric supports, S2, S5 and S10 samples show physical and permeability properties compatible with microfiltration applications. On the other hand, S20 sample exhibit permeability values that are too low to be used as a microfiltration support;
- thanks to geopolymerization, membrane supports for microfiltration can be developed with curing temperatures of 70 °C, allowing for the synthesis of a durable and high-performance material. Compared to ceramic materials used for support preparation, geopolymers therefore do not require heat treatment at high temperatures up to 1200–1800 °C, allowing a considerable reduction in production and environmental costs.

Considering geopolymers promising for the synthesis of sustainable membranes, further research is already ongoing focusing on the deposition of geopolymer selective layers suitable for microfiltration applications. Geopolymer durability is another issue that shall be investigated; however, some literature data are currently available for metakaolin based geopolymer. In terms of chemical resistance, geopolymers are known to suffer the presence of strong acids such as hydrochloric acid and sulphuric acid for prolonged periods of time. In particular, depolymerization of the gel and the formation of zeolites occurs, which can sometimes lead to a strong reduction in mechanical strength [63,64]. Jin et al. [65] showed that immersion in an alkaline solution (NaOH up to pH 13) for 30 days does not lead to a decrease in geopolymer mechanical strength. During membrane cleaning, less aggressive solutions are generally applied for short exposure time, thus highlighting that metakaolin based membrane supports can be attractive as alternative to ceramic materials.

Funding

This research was partially supported by fundamental research funds by University of Bologna.

CRediT author statement

AF: Conceptualization, Investigation, Validation, Writing - Original Draft.

GM: Methodology, Investigation, Validation, Writing-Review & Editing.

SB: Conceptualization, Methodology, Formal analysis, Validation, Writing-Review & Editing.

MB: Conceptualization, Methodology, Validation, Writing-Review & Editing.

Declaration of competing interest

The authors declare that they have no known competing financial interests or personal relationships that could have appeared to influence the work reported in this paper.

Appendix A. Supplementary data

Supplementary data to this article can be found online at https://doi.org/10.1016/j.ceramint.2022.10.233.

References

[1] M. Cheryan, Ultrafiltration and Microfiltration Handbook, CRC Press, 1998, https://doi.org/10.1201/9781482278743.

[2] A.L.Z. Leos, J. Zeman, Microfiltration and Ultrafiltration: Principles and Applications, CRC Press, 2017, https://doi.org/10.1201/9780203747223.

[3] F.L. Gyula Vatai, Erika Bekassy-Molnar, Robert W. Field, Engineering Aspects of Membrane Separation and Application in Food Processing, CRC Press, 2017, https://doi.org/10.4324/9781315374901.

[4] R.W. Baker, Membrane Technology and Applications, John Wiley & Sons Inc, 2012, https://doi.org/10.1002/0470020393.

[5] W. Fan, D. Zou, J. Xu, X. Chen, M. Qiu, Y. Fan, Enhanced performance of fly ash-based supports for low-cost ceramic membranes with the addition of bauxite, Membranes 11 (2021), https://doi.org/10.3390/membranes11090711.

[6] M. Qiu, X. Chen, Y. Fan, W. Xing, 1.11 ceramic membranes, Compr. Membr. Sci. Eng. 1 (2017) 270–297, https://doi.org/10.1016/b978-0-12-409547-2.12243-7.

[7] A. Abdullayev, M.F. Bekheet, D.A.H. Hanaor, A. Gurlo, Materials and applications for low-cost ceramic membranes, Membranes 9 (2019), https://doi.org/10.3390/membranes9090105.

[8] S.L. Sandhya Rani, R.V. Kumar, Insights on applications of low-cost ceramic membranes in wastewater treatment: a mini-review, Case Stud. Chem. Environ. Eng. 4 (2021), 100149, https://doi.org/10.1016/j.cscee.2021.100149.

[9] L. Sun, Z. Wang, B. Gao, Ceramic membranes originated from cost-effective and abundant natural minerals and industrial wastes for broad applications - a review, Desalination Water Treat. 201 (2020) 121–138, https://doi.org/10.5004/dwt.2020.25910.

[10] B. Das, B. Chakrabarty, P. Barkakati, Preparation and characterization of novel ceramic membranes for micro-filtration applications, Ceram. Int. 42 (2016) 14326–14333, https://doi.org/10.1016/j.ceramint.2016.06.125.

[11] D. Khale, R. Chaudhary, Mechanism of geopolymerization and factors influencing its development: a review, J. Mater. Sci. 42 (2007) 729–746, https://doi.org/10.1007/s10853-006-0401-4.

[12] T. Luukkonen, Z. Abdollahnejad, J. Yliniemi, P. Kinnunen, M. Illikainen, One-part alkali-activated materials: a review, Cement Concr. Res. 103 (2018) 21–34, https://doi.org/10.1016/j.cemconres.2017.10.001.

[13] G. Masi, A. Filipponi, M.C. Bignozzi, Fly ash-based one-part alkali activated mortars cured at room temperature: effect of precursor pre-treatments, Open Ceram 8 (2021), 100178, https://doi.org/10.1016/j.oceram.2021.100178.

[14] X. Zhang, C. Bai, Y. Qiao, X. Wang, D. Jia, H. Li, P. Colombo, Porous geopolymer composites: a review, Composer Part A Appl. Sci. Manuf. 150 (2021), 106629, https://doi.org/10.1016/j.compositesa.2021.106629.

[15] A. Filipponi, G. Masi, M.C. Bignozzi, Pressing metakaolin-based one-part geopolymers: influence of the mix design on microstructural and physical properties, Ceram. Int. (2021), https://doi.org/10.1016/j.ceramint.2021.11.129.

[16] N. Ranjbar, A. Kashefi, M.R. Maheri, Hot-pressed geopolymer: dual effects of heat and curing time, Cem. Concr. Compos. 86 (2018) 1–8, https://doi.org/10.1016/j.cemconcomp.2017.11.004.

[17] N. Ranjbar, M. Mehrali, M.R. Maheri, M. Mehrali, Hot-pressed geopolymer, Cement Concr. Res. 100 (2017) 14–22, https://doi.org/10.1016/j.cemconres.2017.05.010.

[18] B. Panda, C. Unluer, M.J. Tan, Extrusion and rheology characterization of geopolymer nanocomposites used in 3D printing, Compos. B Eng. 176 (2019), 107290, https://doi.org/10.1016/j.compositesb.2019.107290.

[19] L. Carabba, R. Moricone, G.E. Scarponi, A. Tugnoli, M.C. Bignozzi, Alkali activated lightweight mortars for passive fire protection: a preliminary study, Construct. Build. Mater. 195 (2019) 75–84, https://doi.org/10.1016/j.conbuildmat.2018.11.005.

[20] J. Zhao, L. Tong, B. Li, T. Chen, C. Wang, G. Yang, Y. Zheng, Eco-friendly geopolymer materials: a review of performance improvement, potential application and sustainability assessment, J. Clean. Prod. 307 (2021), 127085, https://doi.org/10.1016/j.jclepro.2021.127085.

[21] G. Masi, Steel corrosion behavior in light weight fly-ash based Alkali activated mortars, Appl. Sci. 11 (2021) 1–13, https://doi.org/10.3390/app11041908.

[22] E. Kamseu, Z.N.M. Ngouloure, B.N. Ali, S. Zekeng, U.C. Melo, S. Rossignol, C. Leonelli, Cumulative pore volume, pore size distribution and phases percolation in porous inorganic polymer composites: relation microstructure and effective thermal conductivity, Energy Build. 88 (2015) 45–56, https://doi.org/10.1016/j.enbuild.2014.11.066.

[23] S. Chen, S. Ruan, Q. Zeng, Y. Liu, M. Zhang, Y. Tian, D. Yan, Pore structure of geopolymer materials and its correlations to engineering properties: a review, Construct. Build. Mater. 328 (2022), 127064, https://doi.org/10.1016/j.conbuildmat.2022.127064.

[24] C. Bai, P. Colombo, Processing, properties and applications of highly porous geopolymers: a review, Ceram. Int. 44 (2018) 16103–16118, https://doi.org/10.1016/j.ceramint.2018.05.219.

[25] J. ting Wang, Y. yuan Ge, Y. He, M. xue Xu, X. min Cui, A porous gradient geopolymer-based tube membrane with high PM removal rate for air pollution, J. Clean. Prod. 217 (2019) 335–343, https://doi.org/10.1016/j.jclepro.2019.01.268.

[26] Z. Zhang, H. Yu, M. Xu, X. Cui, Preparation, characterization and application of geopolymer-based tubular inorganic membrane, Appl. Clay Sci. 203 (2021), 106001, https://doi.org/10.1016/j.clay.2021.106001.

[27] A. Haris Subaer, A. Irhamsyah, A.D. Permatasari, S.S. Desa, R. Irfanita, S. Wahyuni, Pervaporation membrane based on laterite zeolite-geopolymer for ethanol-water separation, J. Clean. Prod. (2019), 119413, https://doi.org/10.1016/j.jclepro.2019.119413.

[28] J. Zhang, Y. He, Y.P. Wang, J. Mao, X.M. Cui, Synthesis of a self-Supporting faujasite zeolite membrane using geopolymer gel for separation of alcohol/water mixture, Mater. Lett. 116 (2014) 167–170, https://doi.org/10.1016/j.matlet.2013.11.008.

[29] N.A. Ahmad Daud, M.R. Shamsuddin, S.A. Pradanawati, Synthesis and characterization of fly ash-based geopolymer membrane for methylene blue dye removal, IOP Conf. Ser. Earth Environ. Sci. 765 (2021), https://doi.org/10.1088/1755-1315/765/1/012081.

[30] Y. Ge, Y. Yuan, K. Wang, Y. He, X. Cui, Preparation of geopolymer-based inorganic membrane for removing Ni2+ from wastewater, J. Hazard Mater. 299 (2015) 711–718, https://doi.org/10.1016/j.jhazmat.2015.08.006.

[31] H. Chen, Y.J. Zhang, P.Y. He, C.J. Li, H. Li, Coupling of self-supporting geopolymer membrane with intercepted Cr(III) for dye wastewater treatment by hybrid photocatalysis and membrane separation, Appl. Surf. Sci. 515 (2020), 146024, https://doi.org/10.1016/j.apsusc.2020.146024.

[32] Y. He, X. min Cui, X. dong Liu, Y. pin Wang, J. Zhang, K. Liu, Preparation of self-supporting NaA zeolite membranes using geopolymers, J. Membr. Sci. 447 (2013) 66–72, https://doi.org/10.1016/j.memsci.2013.07.027.

[33] P. He, Y. Zhang, H. Chen, X. Zhang, Development of a facile and robust silicomanganese slag-based geopolymer membrane for oil/water separation, Colloids Surfaces A Physicochem. Eng. Asp. 627 (2021), 127072, https://doi.org/10.1016/j.colsurfa.2021.127072.

[34] M. xue Xu, Y. He, C. qun Wang, X. feng He, X. qing He, J. Liu, X. min Cui, Preparation and characterization of a self-supporting inorganic membrane based on metakaolin-based geopolymers, Appl. Clay Sci. 115 (2015) 254–259, https://doi.org/10.1016/j.clay.2015.03.019.

[35] A.K.S. Anu Karthi, L. Cindrella, Self-humidifying novel chitosan-geopolymer hybrid membrane for fuel cell applications, Carbohydr, Polymer 223 (2019), 115073, https://doi.org/10.1016/j.carbpol.2019.115073.

[36] C. Bai, P. Colombo, High-porosity geopolymer membrane supports by peroxide route with the addition of egg white as surfactant, Ceram. Int. 43 (2017) 2267–2273, https://doi.org/10.1016/j.ceramint.2016.10.205.

[37] M. xue Xu, Y. He, Z. han Liu, Z. fa Tong, X. min Cui, Preparation of geopolymer inorganic membrane and purification of pulp-papermaking green liquor, Appl. Clay Sci. 168 (2019) 269–275, https://doi.org/10.1016/j.clay.2018.11.024.

[38] C. Finocchiaro, G. Barone, P. Mazzoleni, C. Leonelli, A. Gharzouni, S. Rossignol, FT-IR study of early stages of alkali activated materials based on pyroclastic deposits (Mt. Etna, Sicily, Italy) using two different alkaline solutions, Construct. Build. Mater. 262 (2020), 120095, https://doi.org/10.1016/j.conbuildmat.2020.120095.

[39] H. Wang, H. Li, F. Yan, Synthesis and mechanical properties of metakaolinite-based geopolymer, Colloids Surfaces A Physicochem. Eng. Asp. 268 (2005) 1–6, https://doi.org/10.1016/j.colsurfa.2005.01.016.

[40] P. Rovnaník, Effect of curing temperature on the development of hard structure of metakaolin-based geopolymer, Construct. Build. Mater. 24 (2010) 1176–1183, https://doi.org/10.1016/j.conbuildmat.2009.12.023.

[41] T. Luukkonen, M. Sarkkinen, K. Kemppainen, J. Rämö, U. Lassi, Metakaolin geopolymer characterization and application for ammonium removal from model solutions and landfill leachate, Appl. Clay Sci. 119 (2016) 266–276, https://doi.org/10.1016/j.clay.2015.10.027.

[42] V.F.F. Barbosa, K.J.D. MacKenzie, C. Thaumaturgo, Synthesis and characterisation of materials based on inorganic polymers of alumina and silica: sodium polysialate polymers, Int. J. Inorg. Mater. 2 (2000) 309–317, https://doi.org/10.1016/S1466-6049(00)00041-6.

[43] Z. Li, S. Zhang, Y. Zuo, W. Chen, G. Ye, Chemical deformation of metakaolin based geopolymer, Cement Concr. Res. 120 (2019) 108–118, https://doi.org/10.1016/j.cemconres.2019.03.017.

[44] J.N. Yankwa Djobo, A. Elimbi, H.K. Tchakouté, S. Kumar, Mechanical activation of volcanic ash for geopolymer synthesis: effect on reaction kinetics, gel characteristics, physical and mechanical properties, RSC Adv. 6 (2016) 39106–39117, https://doi.org/10.1039/c6ra03667h.

[45] M. Cyr, R. Pouhet, Carbonation in the pore solution of metakaolin-based geopolymer, Cement Concr. Res. 88 (2016) 227–235, https://doi.org/10.1016/j.cemconres.2016.05.008.

[46] R. Pouhet, M. Cyr, R. Bucher, Influence of the initial water content in flash calcined metakaolin-based geopolymer, Construct. Build. Mater. 201 (2019) 421–429, https://doi.org/10.1016/j.conbuildmat.2018.12.201.

[47] D.O. Obada, D. Dodoo-Arhin, M. Dauda, F.O. Anafi, A.S. Ahmed, O.A. Ajayi, Physico-mechanical and gas permeability characteristics of kaolin based ceramic membranes prepared with a new pore-forming agent, Appl. Clay Sci. 150 (2017) 175–183, https://doi.org/10.1016/j.clay.2017.09.014.

[48] S. Bouzid Rekik, J. Bouaziz, A. Deratani, S. Baklouti, Study of ceramic membrane from naturally occurring-kaolin clays for microfiltration applications, Period. Polytech. - Chem. Eng. 61 (2017) 206–215, https://doi.org/10.3311/PPch.9679.
[49] M.M. Lorente-Ayza, S. Mestre, M. Menéndez, E. Sánchez, Comparison of extruded and pressed low cost ceramic supports for microfiltration membranes, J. Eur. Ceram. Soc. 35 (2015) 3681–3691, https://doi.org/10.1016/j.jeurceramsoc.2015.06.010.
[50] I. Jedidi, S. Khemakhem, A. Larbot, R. Ben Amar, Elaboration and characterisation of fly ash based mineral supports for microfiltration and ultrafiltration membranes, Ceram. Int. 35 (2009) 2747–2753, https://doi.org/10.1016/j.ceramint.2009.03.021.
[51] F. Aouadja, F. Bouzerara, C.M. Guvenc, M.M. Demir, Fabrication and properties of novel porous ceramic membrane supports from the (Sig) diatomite andalumina mixtures, Bol. La Soc. Esp. Ceram. y Vidr. (2021) 1–10, https://doi.org/10.1016/j.bsecv.2021.04.002.
[52] H. Qi, Y. Fan, W. Xing, L. Winnubst, Effect of TiO2 doping on the characteristics of macroporous Al2O3/TiO2 membrane supports, J. Eur. Ceram. Soc. 30 (2010) 1317–1325, https://doi.org/10.1016/j.jeurceramsoc.2009.12.011.
[53] X. Yin, K. Guan, P. Gao, C. Peng, J. Wu, A preparation method for the highly permeable ceramic microfiltration membrane-precursor film firing method, RSC Adv. 8 (2018) 2906–2914, https://doi.org/10.1039/c7ra12314k.
[54] Y. Dong, B. Lin, J.E. Zhou, X. Zhang, Y. Ling, X. Liu, G. Meng, S. Hampshire, Corrosion resistance characterization of porous alumina membrane supports, Mater. Char. 62 (2011) 409–418, https://doi.org/10.1016/j.matchar.2011.01.012.
[55] W. Qin, C. Peng, J. Wu, A sacrificial-interlayer technique for single-step coating preparation of highly permeable alumina membrane, Ceram. Int. 43 (2017) 901–904, https://doi.org/10.1016/j.ceramint.2016.09.206.
[56] Y.H. Wang, Y. Zhang, X.Q. Liu, G.Y. Meng, Microstructure control of ceramic membrane support from corundum-rutile powder mixture, Powder Technol. 168 (2006) 125–133, https://doi.org/10.1016/j.powtec.2006.07.010.
[57] W. Qin, Y. Zhang, J. Wu, Preparation of high-permeance ceramic microfiltration membranes using a pore-sealing method, RSC Adv. 10 (2020) 5560–5565, https://doi.org/10.1039/c9ra09805d.
[58] C. Kuenzel, L.J. Vandeperre, S. Donatello, A.R. Boccaccini, C. Cheeseman, Ambient temperature drying shrinkage and cracking in metakaolin-based geopolymers, J. Am. Ceram. Soc. 95 (2012) 3270–3277, https://doi.org/10.1111/j.1551-2916.2012.05380.x.
[59] N. Ranjbar, M. Mehrali, A. Behnia, A.J. Pordsari, M. Mehrali, U.J. Alengaram, M. Z. Jumaat, A comprehensive study of the polypropylene fiber reinforced fly ash based geopolymer, PLoS One 11 (2016), https://doi.org/10.1371/journal.pone.0147546.
[60] N. Ranjbar, A. Kashefi, G. Ye, M. Mehrali, Effects of heat and pressure on hot-pressed geopolymer, Construct. Build. Mater. 231 (2020), 117106, https://doi.org/10.1016/j.conbuildmat.2019.117106.
[61] Y. Huang, Z. Yang, Y. He, X. Wang, An overview on nonlinear porous flow in low permeability porous media, Theor. Appl. Mech. Lett. 3 (2013), 022001, https://doi.org/10.1063/2.1302201.
[62] B. Ghouil, A. Harabi, F. Bouzerara, B. Boudaira, A. Guechi, M.M. Demir, A. Figoli, Development and characterization of tubular composite ceramic membranes using natural alumino-silicates for microfiltration applications, Mater. Char. 103 (2015) 18–27, https://doi.org/10.1016/j.matchar.2015.03.009.
[63] T. Bakharev, Resistance of geopolymer materials to acid attack, Cement Concr. Res. 35 (2005) 658–670, https://doi.org/10.1016/j.cemconres.2004.06.005.
[64] Y. Aygörmez, O. Canpolat, Long-term sulfuric and hydrochloric acid resistance of silica fume and colemanite waste reinforced metakaolin-based geopolymers, Rev. La Constr. 20 (2021) 291–407, https://doi.org/10.7764/RDLC.20.2.72.
[65] M. Jin, Z. Zheng, Y. Sun, L. Chen, Z. Jin, Resistance of metakaolin-MSWI fly ash based geopolymer to acid and alkaline environments, J. Non-Cryst. Solids 450 (2016) 116–122, https://doi.org/10.1016/j.jnoncrysol.2016.07.036.